Final Draft
of the original manuscript:

Xu, L.; Willumeit-Roemer, R.; Luthringer-Feyerabend, B.J.C.:
Effect of magnesium-degradation products and hypoxia on the angiogenesis of human umbilical vein endothelial cells.
In: Acta Biomaterialia. Vol. 98 (2019) 269 - 283.
First published online by Elsevier: 19.02.2019

https://dx.doi.org/10.1016/j.actbio.2019.02.018

Effect of magnesium-degradation products and hypoxia on the angiogenesis of human umbilical vein endothelial cells ✯

Lei Xu, Regine Willumeit-Römer, Bérengère J.C. Luthringer-Feyerabend*

Institute of Materials Research, Division for Metallic Biomaterials, Helmholtz-Zentrum Geesthacht (HZG), Geesthacht, Germany

* Corresponding author: Bérengère J.C. Luthringer-Feyerabend, Berengere.Luthringer@HZG.de

Footnote: ✯ Part of the Special Issue associated with the 10th International Conference on Biodegradable Metals, 10th Biometal 2018, held at the University of Oxford, 26-31 Aug. 2018, organized by Professors Diego Mantovani and Frank Witte.

Abstract:

Biodegradable magnesium (Mg) metals have been applied in orthopaedic and stent applications due to their biodegradability, bioabsorbability and adaptability to tissue regeneration. However, further investigations are still needed to understand how angiogenesis will respond to high concentrations of Mg^{2+} and oxygen content differences, which are vital to vascular remodelling and bone fracture regeneration or tissue healing. Human primary endothelial cells were exposed to various concentrations (2 to 8 mM) of extracellular Mg^{2+} degradation products under either hypoxia or normoxia. Increased proliferation was measured with Mg extracts under hypoxia but not under normoxia. Under normoxia and with Mg extracts, HUVEC migration exhibited a bell-shaped curve. The same pattern was observed with VEGFB expression, while VEGFA was constantly downregulated. Under hypoxia, migration and VEGFA levels remained constant; however, VEGFB was upregulated. Similarly, under normoxia, tube formation as well as VEGFA and VEGFB levels were downregulated. Nevertheless, under hypoxia, tube formation remained constant while VEGFA and VEGFB levels were upregulated. These results suggest that Mg extracts did not interfere with angiogenesis under hypoxia.

Statement of significance

Neoangiogenesis, mediated by (*e.g.*) hypoxia, is a key factor for proper tissue healing Thus, effect of Mg^{2+} degradation products under either hypoxia or normoxia on angiogenesis were investigated. Under normoxia and increased Mg concentrations, a general negative effect was measured on early (migration) and late (tubulogenesis) angiogenesis. However, under hypoxia, this effect was abolished. As magnesium degradation is an oxygen-dependant process, hypoxia condition may be a relevant factor to test material cytocompatibility *in vitro*.

Keywords: magnesium; hypoxia; normoxia; primary endothelial cell; angiogenesis

Introduction

Angiogenesis defines the formation of new blood vessels ranging from large arteries to micron-sized capillaries. Intussusceptive and sprouting angiogenesis are the two types of angiogenesis. Intussusceptive (or splitting) angiogenesis is generally a fast process that relies on the remodelling of existing vessels splitting into two [1]. In contrast, sprouting angiogenesis depends on endothelial cell proliferation or migration. This process can be divided in the following different steps: (i) enzymatic degradation of the capillary basement membrane in existing blood vessels to allow endothelial cells to escape; (ii) endothelial cell proliferation and directed migration towards a source signal; and (iii) reorganisation through tubulogenesis (endothelial cell tube formation), vessel fusion, vessel pruning, and pericyte stabilisation.

Angiogenesis has been investigated for the optimisation of vascular stents because proper endothelialisation of larger vessels is critical to avoid stent failure from thrombosis and intimal hyperplasia [2]. In pathology, angiogenesis is also a fundamental step in tumour transition, in which endothelial cells respond to tumour-secreted angiogenic signals by stimulating the growth of new blood vessels to receive cytokines, oxygen and nutrients [3]. In addition to angiogenesis, wound hypoxia also has a critical role in the fate of the normal healing process. Hypoxia has been proven a vital factor in the wound environment because the lack of oxygen induced by blood clotting notably mediates (sprouting) angiogenesis [4]. Indeed, the expression of several angiogenic genes are regulated through the hypoxia inducible factor (HIF)/VEGF signalling axis, where oxygen is an important signalling molecule [5]. The angiogenesis process comes into play rather early during wound healing. It is commonly admitted that during the first 2 to 5 days after tissue damage, the clotting cascade is taking place accompanied with an inflammatory environment. Directly after this process, under normal conditions, angiogenesis should occur to provide an adequate supply of oxygen, nutrients, growth factors, and cells. This return to nonmedia in turn promotes the proliferation/granulation phase.

As a promising biomaterial, we have been investigating magnesium (Mg) and developing its alloys since the material's biodegradability can prevent second surgeries and its biocompatibility can stimulate cell metabolism and proliferation. Some reports have revealed the mechanism of the Mg ion on endothelial cells. For instance, Mg^{2+} can interplay with adenosine diphosphate (ADP), adenosine triphosphate (ATP) and the mitochondria in the cytosol. Moreover, it has been proven that Mg material can induce variations in the Mg ion concentration compared to physiological conditions, and Mg can influence the migration phase of angiogenesis [6]. These studies indicating the roles of Mg were mostly performed with hypomagnesemia models, but mechanistic studies and evidence are still sparse and general [7]. Furthermore, degradation of magnesium (alloys) materials requires oxygen, which could in turn further influence angiogenesis and healing [8].

Angiogenesis is a stage-dependent process that initially involves endothelial cell migration into relevant areas followed by the formation of tubular structures. Greater understanding of the angiogenesis mechanisms in the presence of Mg and hypoxia can shed light on the design of Mg-based implants or stents and their tailored degradation rate. Therefore, the influence of Mg was studied with a human umbilical vein endothelial cell (HUVEC) model. A high purity isolated endothelial population from the endothelium layer of a human umbilical cord was validated by flow cytometry. Furthermore, to mimic different healing times, hypoxic conditions were induced using 5% oxygen and normoxia using 20% oxygen [9]. The two stages of angiogenesis, including migration (*via* wound healing assay) and vessel or tube formation (*i.e.*, the ability to form capillary-like structures), were studied not only at the phenotypic level but also at the gene level. Finally, vascular endothelial growth factor B (VEGFB), a strong angiogenic factor, was also measured at the protein level to clarify on the mechanism of Mg on endothelial cell migration and tube formation abilities.

Material and methods

HUVEC isolation, culture, and immunophenotyping

Ethical approval for the isolation of HUVECs was obtained from the Ethik-Kommission der Ärztekammer, Hamburg. Umbilical cord samples were provided by Asklepios Klinik Altona (Hamburg, Germany) immediately after caesarean sections of consenting donors. HUVEC isolation from a human umbilical vein was adapted from a previously reported method [10] using 0.2% (w/v) collagenase (from *Clostridium histolyticum* Type IA; Sigma Aldrich, Munich, Germany). Isolated HUVECs and commercial HUVEC products (selected as control - BD™ HUVEC-2, BD Bioscience, Heidelberg, Germany) were cultured in endothelial cell growth medium (ECGM, PromoCell, Heidelberg, Germany) supplemented with endothelial cell growth supplement (ECGS, PromoCell, Heidelberg, Germany) and 10% foetal bovine serum (FBS, Biochrom, Berlin, Germany). The cell identity was confirmed according to the expression of specific markers (Supplementary Table S1; positive control cluster of differentiation (CD) 31 and CD105 – negative control CD45) and corresponding isotype controls (all antibodies were purchased from Fisher Scientific GmbH, Schwerte, Germany) by flow cytometry (S3e Cell Sorter; Bio-Rad Laboratories GmbH, Munich, Germany). Cells were dissociated with 0.05% trypsin-EDTA (Life Technologies GmbH, Darmstadt, Germany). The dissociated cells were stained with fluorescein isothiocyanate (FITC)-conjugated mouse anti-human CD105 monoclonal, PE-labelled mouse anti-human CD31 monoclonal, or FITC-labelled mouse anti-CD45 monoclonal antibodies or corresponding isotypes (mouse immunoglobulin G) added to the cell suspension in phosphate-buffered saline (PBS) containing 1% bovine serum albumin (BSA; Carl Roth GmbH, Karlsruhe, Germany). Samples were incubated at 4°C for 30 min in dark and analysed by fluorescence label 1 (FL1) or FL2. The positive expression was obtained by gating 95% of the event isotype control results and then inverting the gate to obtain a percentage of positively stained cells in the samples using the ProSort software (version 1.6; Bio-Rad Laboratories GmbH, Munich, Germany). After sufficient expansion, cells were further cultured with alpha minimum essential medium (α-MEM, Invitrogen - Fisher Scientific GmbH, Schwerte, Germany) supplemented with 15% FBS for human mesenchymal stem cells (hMSC-FBS, Biological

Industries, Israel) and 1% penicillin streptomycin (P/S, Life Sciences, Karlsruhe, Germany). HUVECs were used up to passage 6.

Magnesium extract

Pure Mg (Pure-Mg, 99.95%) was prepared by permanent mould gravity casting (Helmholtz Zentrum Geesthacht, Geesthacht, Germany). After T4 treatment, ingots were extruded into 1.2-cm diameter rods and machined to obtain a diameter of 1 cm. Finally, 1.5-mm thickness discs were cut. The discs were cleaned *via* 20 min sonication in 100% n-hexane, 100% acetone, and 100% ethanol; sterilised in 70% ethanol (Merck, Darmstadt, Germany); and further dried on a clean bench. Mg-degradation products or extracts were produced according to EN ISO standards I. 10993-5:2009 and I. 10993-12:2012 (0.2 g material/mL extraction medium). Next, the discs were incubated in HUVEC cell culture medium (*i.e.*, α-MEM, 15% hMSC-FBS, and 1% P/S) for 72 h under physiological conditions (5% CO_2, 20% O_2, 95% relative humidity, and 37 °C) in an incubator (Heraeus BB 6220, Thermo Scientific - Fisher Scientific GmbH, Schwerte, Germany). Afterwards, the Mg, Ca and phosphorous (P) contents were measured (Supplementary Table S2) *via* inductively coupled plasma mass spectrometry (ICP-MS; Agilent 7700x ICP-MS, Waldron, Germany). The Mg extract was diluted to 2, 4, and 8 mM with α-MEM plus 15% hMSC-FBS and 1% P/S. The osmolality and pH of the diluted extractions were tested using a Gonotec 030-D cryoscopic osmometer (Gonotec, Berlin, Germany) and an ArgusX pH Meter (Sentron Europe BV, Roden, the Netherlands), respectively (Table S2).

Proliferation

Proliferation was assessed by measuring DNA quantification. In total, 10,000 HUVEC per well were seeded in 24-well plates in 0.5 mL of Mg extract solution or α-MEM medium (as the control) at 37°C with either 20% or 5% O_2 for 24 h. The HUVECs were lysed by lysis buffer (25 mM NaOH and 0.2 mM EDTA) and incubated for 5 min at 37°C. The lysate was incubated at 98°C for 1 h with 1,000 rpm rotation and reduced to 15°C at 700 rpm. Neutralisation buffer was then added (40 mM Tris/HCl pH 5.5) and the samples were centrifuged at 13,000 rpm for 1 min. The samples were diluted 1:5 in DNA dilution buffer (2.5 M NaCl in 19 mM sodium citrate at pH 7). Moreover, 100 µL of diluted samples and 50 µL of DNA working buffer (2 M NaCl in 15 mM sodium citrate pH 7) as well as 50 µL of bisbenzimide solution (2 µg/mL bisbenzimide in DNA Working Buffer) were pipetted into a 96-well plate in triplicate and incubated for 15 min in the dark. The DNA content was quantified based on bisbenzimide fluorescence in NaCl and sodium citrate solution (pH 7 with HCl) with a VICTOR3 multilabel plate reader (Perkin Elmer, Massachusetts, USA) at an excitation wavelength of 355 nm and an emission wavelength of 460 nm. The DNA concentration was calculated using the fluorescence values in the standard curve.

Metabolism (WST-1) assay

HUVECs (10,000 cells/per well in 24-well plate) were cultured without (control) or with various concentrations of Mg degradation products at 37 °C in 20% and 5% O_2 for 24 h. Afterwards, the media

was exchanged with 0.5 mL of fresh α-MEM complete medium supplemented with 50 µL of WST-1 (PreMix WST-1 Cell Proliferation Assay System; Takara Bio Inc., Shiga, Japan) for 30 min in an incubator (with either 20% or 5% O_2) to monitor the metabolism by the cleavage of the tetrazolium salt. The absorbance of 100 µL of each sample was measured in triplicate using a microplate reader (Sunrise™ Tecan, Tecan Deutschland GmbH, Crailsheim, Germany) at 450 nm. The absorbance was normalised by the DNA content from the DNA quantification.

Mitochondrial membrane potential (Δψm) assay

HUVECs were seeded at 10,000 cells per well in 24-well plates and cultured with Mg degradation products and α-MEM (as control) at 37°C in 20% and 5% O_2. After 24 h culture, 30 nM digitonin (Carl Roth GmbH, Karlsruhe, Germany) was added to each well and incubated for 5 min on ice to selectively permeabilise the plasma membrane [11]. Rhodamine 123 (R123; Sigma-Aldrich Chemie GmbH, Munich, Germany) was added (10 µg/mL in PBS) to each well and then incubated for 10 min at room temperature (RT). R123 was excited (λ_{Ex}) at 510 nm and the fluorescence emission was detected at (λ_{Em}) 534 nm with a VICTOR3 multilabel plate reader (Perkin Elmer, Rodgau, Germany). Antimycin A (Sigma-Aldrich Chemie GmbH, Munich, Germany) was added (10 µM) to the cells for 1 min and afterwards the fluorescence was measured every 2 min three times.

Wound healing assay

HUVECs were seeded in 24-well plates, cultured until reaching 80% confluence, and then starved in ECGM complete medium without extra FBS for 24 h. To avoid any interference from cell proliferation in this assay, the HUVECs were treated with 10 µg/mL mitomycin C (from *Streptomyces*, Sigma-Aldrich Chemie GmbH, Munich, Germany) for 2 h. Mitomycin C acts as a double-stranded DNA alkylating agent that inhibits DNA synthesis and cell proliferation. A cell monolayer was scratched with a 1 mL pipet tip to achieve “wounds”. Images were immediately collected and labelled controls (0 h). The wounds were cultured with Mg degradation dilutions in α-MEM under physiological or hypoxia conditions for 24 h and then stained with Calcein AM at 37 °C for 30 min. Images were once again acquired with an inverted microscope and labelled treated values (24 h). Images were analysed with ImageJ with the MRI Wound Healing Tool (MRI’s Redmine). The wound healing closure was calculated as the scratch area differences between 0 h and 24 h.

Tube formation assay

Each well (24-well plates) was first coated with 10 µL of matrix (Geltrex® LDEV-Free Reduced Growth Factor Basement Membrane Matrix, Fisher Scientific GmbH, Schwerte, Germany) by homogeneously pouring and spreading with the tip of the 1 mL combitip nozzle (Eppendorf AG, Hamburg, Germany). The matrix was allowed to polymerise at 37°C for 30 min. On this reconstituted matrix, 4.0×10^4 HUVECs were cultured in α-MEM complete medium (as control) or Mg degradation products under physiological or hypoxia conditions (20% and 5% oxygen, respectively) for 6 h. The tubes were then stained with

Calcein AM (Invitrogen - Fisher Scientific GmbH, Schwerte, Germany) diluted 1:5,000 in PBS at 37 °C for 30 min. Afterwards, microphotographs were taken with an inverted microscope (Eclipse Ti, Nikon GmbH, Düsseldorf, Germany). The images were analysed with the ImageJ software (v.1.51b, Rasband, W.S., ImageJ, U.S. National Institutes of Health, Bethesda, Maryland, USA, https://imagej.nih.gov/ij/, 1997-2016) with the Angiogenesis Analyser Plugin (Gilles Carpentier Research). The total length of the tubes and number of branches were quantified.

Ribonucleic acids (RNA) extraction and real-time polymerase chain reaction (RT-qPCR)

RNA from two independent experiments from two donors from the tube formation and wound healing assays were extracted using the Qiagen RNeasy Mini kit and Qiagen shredder (Qiagen, Hilden, Germany) following the manufacturer's protocol. RNA concentrations (optical density (OD) at 260 nm) and purity (OD at 260/280 nm) were measured using a NanoDrop 2000c (Thermo Scientific - Fisher Scientific GmbH, Schwerte, Germany). Complementary deoxyribonucleic acid (cDNA) was synthesised with the Omniscript Reverse Transcription Kit (Qiagen, Hilden, Germany). Primers (Supplementary Table S3) were designed by Primer 3 (version 4.0.0) or found in the RTPrimerDB database and purchased from Eurofins NDSC Food Testing Germany GmbH (Hamburg, Germany). Glyceraldehyde-3-phosphate dehydrogenase (GAPDH), beta-2-microglobulin (B2M) and actin beta (β-actin) were used as reference genes. RT-qPCR were performed in triplicate using SsoFast™ EvaGreen® Supermix (Bio-Rad Laboratories GmbH, Munich, Germany) with a CFX96 Touch real-time PCR detection system and the CFX Manager software (version 3.1, Bio-Rad Laboratories GmbH, Munich, Germany). The thermal cycling conditions consisted of an initial denaturation at 95°C for 3 min, followed by 40 cycles of 20 s of denaturation at 95°C, 20 s of annealing at 60°C, and 30 s of elongation at 75°C. A melting curve step (30 s at 95°C from 65 to 95°C with 0.5°C increments for 5 s) was added to confirm the melting temperatures (Tm) of the PCR products. All samples and non-treatment-controls were run in duplicate. The quantification of gene expression was performed using the comparative CT (ΔC(t) and ΔΔC(t)) method, and it is reported as the fold difference relative to internal controls and target mRNA relative to the control sample (set to 1).

Enzyme-linked immunosorbent assay (ELISA)

In the tube formation and wound healing assays, 500 µL of medium from each group was collected and centrifuged (2,000 rpm, 2 min) to obtain supernatants. Quantification of VEGFA and VEGFB concentrations was performed using a colorimetric sandwich ELISA assay. The supernatant for VEGFA quantification was diluted 1:4 (DY293, R&D systems, Germany). According to the manufacturer, the supernatant for VEGFB was diluted 1:1 (RAB1095, Sigma Aldrich, Germany). To ensure the specific primary antibody-antigen-secondary antibody binding, nonspecific results were reduced by washing the non-bound antibody from the bound materials with an autowasher (Bio-Plex Pro™ wash station; Bio-Rad Laboratories GmbH, Munich, Germany). The optical density (OD) was read at 450 nm using a microplate reader (Sunrise™ Tecan, Tecan Deutschland GmbH, Crailsheim, Germany).

Statistical analysis

The qRT-PCR data represent the results from two independent experiments with two replicates from two donors. Other results were collected from three independent experiments with two replicates for three donors. All data were presented as the average with standard deviation (SD). Either one-way ANOVA or one-way ANOVA on ranks was performed based on the distribution of the data using SigmaPlot (version 13.0; Systat software GmbH, Erkrath, Germany). The post-hoc multiple comparisons were based on the Tukey test (α=0.05). For RT-qPCR, to detect the differential expression, a *t*-test ($P<0.05$) was employed and directly calculated using the CFX Manager Software (version 3.0; Bio Rad, Munich, Germany).

Results:

HUVEC immunophenotyping

The $CD31^+$ and $CD105^+$ populations of isolated HUVECs were 99.637% and 94.67%, respectively. Compared to validated purchased HUVECs and isotype controls, the isolated HUVEC presented a highly positive ratio (Fig. 1) and showed a similar “cobblestone” morphology (Supplemental Fig. S1).

Proliferation

DNA content is correlated to cell number and thus proliferation. No significant changes in the DNA contents were measured with Mg at 20% O_2. However, under 5% O_2, HUVECs cultured with 4 and 8 mM Mg degradation products exhibited increased DNA contents compared to the control (Fig. 2a). According to a multiple comparison (Fig. 2b), cells at 4 and 8 mM Mg under hypoxia had higher DNA contents than the cells measured with different concentrations of Mg at 20% O_2 (except 4 mM 5% vs. Ctr 20%).

Metabolism assay

The tetrazolium salt WST-1 (4-[3-(4-iodophenyl)-2-(4-nitrophenyl)-2H-5-tetrazolio]-1,3-benzene disulfonate) can be cleaved into formazan dye, which can in turn quantitatively represent the metabolic activity of cells. By normalising the results from the WST-1 and R123 assays with DNA content, *i.e.*, cell number, the results enable the comparison of the influence of the magnesium degradation products on HUVEC metabolism. Under 5% O_2, statistically significant decreases in WST-1 can be seen with 4 and 8 mM Mg compared to the control, as well as between 2 and 8 mM Mg (Fig. 3a). To measure the influence of Mg-degradation products and O_2 contents on mitochondrial membrane energization, the mitochondrial membrane potential gradient was measured. Adenosine triphosphate (ATP) synthesis by F_0F_1ATPase during cellular respiration originates from an electrochemical gradient created by the difference in the proton (H^+) concentration across the mitochondrial membrane (*i.e.*, potential). Quenching of R123 fluorescence is induced by inhibiting mitochondrial energisation; thus, it is possible to measure $\Delta\Psi M$ as it is proportional to the fluorescence decay [12]. R123 is a fluorescent cationic dye

that can bind to the mitochondria and other plasma membranes. Digitonin can increase the sensitivity of R123 probes by permeabilising the cell plasma membrane and allowing access to the inner membrane [13]. Antimycin A, an inhibitor of complex III in the respiratory chain, can rapidly collapse the energy-linked absorbance [14]. Therefore, the combination of digitonin, R123 and antimycin A can assess mitochondrial energisation in intact cells by excluding non-mitochondrial staining by subtracting the fluorescence after antimycin A treatment (Fig. 3d). HUVECs treated with 2 and 4 mM Mg at 20% O_2 indicated significantly higher R123 retention (compared to the control). However, under 5% O_2, all Mg doses showed decreased effects on Δψm (Fig. 3d).

Wound healing assay

Wound closure was calculated from the difference in scratch areas between the 0 and 24th h to assess the influence of Mg on cell migration. Under 5% O_2 and compared to the 5% control, Mg-degradation products had no influence on the closure area or cell migration (Fig. 4). However, cell migration was increased with Mg at 20% O_2 (significantly with 2 mM compared to control 20%). A bell-shaped curve, *i.e*., increased migration at low concentrations of Mg extract and decreased at high concentrations, may be observed.

To explore the potential gene regulation influenced by the Mg degradation products and hypoxia during HUVEC migration, specific gene expression was studied. Significantly regulated genes are presented in Table 1. Under 5% O_2, most of the selected genes were downregulated, but not in a dose-dependent manner. These results are in accordance with the phenotypic observations during wound healing (*i.e*., no effect observed under hypoxia and increased Mg extract concentrations). Under 20% O_2, fewer genes were regulated. However, it is interesting to notice that the previously observed bell-shaped curve for wound healing can be related to some gene expression. Indeed, some genes (*e.g*., vascular endothelial growth factor B isoform (VEGFB186) and interleukin 8 (IL8 or chemokine (C-X-C motif) ligand 8, CXCL8)) exhibited increased and then decreased expression together with the increased concentrations of Mg. Other genes such as angiogenin (ANG) and tissue inhibitors of metalloproteinase 1 (TIMP1) were upregulated only at 2 mM. To exhaustively describe the results and highlight the potential relationships, the regulated genes were classified into the following 6 groups:

i. **Cell surface and cytoskeleton organisation.** Under 20% O_2, ANG and ezrin (EZR) were upregulated by 2 mM Mg. Vascular cell adhesion protein 1 (VCAM1) was upregulated by 4 mM Mg. VEGFB186 and vascular endothelial growth factor receptor 1 (FLT1) were upregulated by 2 and 4 mM but downregulated by 8 mM Mg. Vascular endothelial growth factor receptor 2 (KDR) was upregulated at 2 and 4 mM Mg. Transmembrane 4 (CD9) was upregulated by 2 mM Mg but downregulated by 8 mM Mg. At 5% O_2, all of these genes were increasingly downregulated from 2 to 8 mM Mg.
ii. **Adhesion.** Integrin subunit alpha 2 (ITGA2) and integrin subunit alpha M (ITGAM) were upregulated by 2 mM Mg, but ITGA2 was also downregulated by 8 mM Mg at 20% O_2. Under

hypoxia, ITGA2 was downregulated from 2 to 8 mM Mg and ITGAM was downregulated at 2 and 4 mM Mg.

iii. **Migration and preconditions for vessels.** At 20% O_2, IL8 was upregulated at 2 and 4 mM Mg and downregulated by 8 mM Mg. Matrix metallopeptidase 13 (MMP13) was upregulated at 2 and 4 mM Mg. TIMP1 was upregulated at 2 mM Mg. Under hypoxia, IL8, MMP13 and TIMP1 were all downregulated under the influence of 2 to 8 mM Mg.

iv. **HUVEC differentiation and hypoxia sensor.** Basic fibroblast growth factor (FGF2), hypoxia-inducible factor 1 alpha subunit (HIF1A) and interferon gamma (IFNγ) were upregulated under 2 mM Mg at 20% O_2; however, they were downregulated by Mg at 5% O_2. HIF2A was downregulated at 8 mM Mg under 20% O_2 and under hypoxia at 2 to 8 mM Mg. The IFNγ was upregulated by 2 mM Mg at 20% O_2 but downregulated by 2 and 4 mM Mg in 5% O_2.

v. **Ca^{2+}, Mg^{2+} flux, cell mobility and blood vessel diameter.** Ca-activated neutral protease 1 (CAPN1) was observed to be initially upregulated at 20% O_2 with 2 mM Mg but remarkably downregulated with up to 8 mM Mg at 5% O_2. Claudin 16 (CLD16) was significantly downregulated under hypoxia.

vi. **Vascular protection and adaptive effect.** Nitric oxide synthase (NOS2) was upregulated at 20% O_2 by significantly downregulated with 2 and 4 mM Mg at 5% O_2.

Tube formation

An obvious reduction in the total length of tubes and number of branches at 4 and 8 mM Mg (Fig. 5b and 5c) was observed at 20% O_2 after 6 h. However, under 5% O_2, there were no significant changes. Post hoc tests did not indicate significance induced by Mg between 20% and 5% O_2.

The regulation of selected genes during tube formation as influenced by Mg degradation products and O_2 contents were also investigated. Specific targets (Table S3) were tested and significant changes are presented in Table 2. In tube formation, only ANG and ITGA3 were upregulated by Mg degradation products under 20% O_2; however, 11 genes were downregulated. Under hypoxia, downregulation was tempered and four genes were even upregulated. Only MMP13 was downregulated at 5% O_2. Once again, the remarkably regulated genes were classified into the following 6 classes:

i. **Cell surface and cytoskeleton organisation.** Under 5% O_2, no obvious regulation of ANG was observed, though there was significant upregulation by 2 mM Mg at 20% O_2. VEGFB186 was downregulated at 20% O_2 by 4 and 8 mM Mg but upregulated at 5% O_2 with 8 mM Mg. Both FLT1 and KDR were downregulated at 20% O_2 by 4 and 8 mM Mg and upregulated at 2 mM Mg under hypoxia. No significant regulation of CD9 and EZR were observed under hypoxia. CD9 was downregulated at 20% O_2 by 4 and 8 mM Mg. EZR was also downregulated by 4 Mm Mg at 20% O_2.

ii. **Adhesion.** Mg extract did not influence the expression of ITGA2 and ITGAM at either 20% or 5% O_2. ITGA3 was upregulated by 2 mM Mg at 20%.

iii. **Migration and precondition for vessels.** IL8 and MMP13 were downregulated by 4 mM Mg degradation products at 20% and 5% O_2. TIMP1 was remarkably downregulated by 4 and 8 mM Mg degradation products.

iv. **HUVEC differentiation and hypoxia sensor.** Both HIF1A and HIF2A expression were upregulated by 2 mM Mg but downregulated by 4 mM Mg at 20% O_2. In contrast, HIF1A was downregulated by 4 mM Mg and upregulated by 8 mM Mg under hypoxia. IFNγ was downregulated by 4 mM Mg at 20% O_2.

v. **Ca^{2+}, Mg^{2+} flux, cell mobility and blood vessel diameter.** CAPN1 and CLD16 were downregulated by 4 and 8 mM Mg at 20% O_2.

vi. **Vascular protection and adaptive effect.** NOS2 was downregulated by 4 and 8 mM Mg at 20% O_2.

VEGFA and VEGFB levels (ELISA test)

To determine whether the influence of Mg treatments and oxygen conditions on capillary formation and the migration process is mediated through VEGFA and/or VEGFB, two angiogenic factors from the VEGF family, their concentrations were quantified in the supernatants from the wound healing and tube formation experiments.

For wound healing and tube formation, no differences could be observed under hypoxia. However, under normoxia, a decrease could be detected for wound healing in Fig. 6a in a dose-dependent manner (statistically significant decreases for 8 mM vs. Ctr and 2 mM). For tube formation, approximately the same level of statistically significant downregulation could be detected for all the Mg concentrations vs. the Ctr (Fig. 6b). During wound healing (Fig. 6c), a decrease and an increase in VEGFB levels were observed in a dose-dependent manner for normoxia and hypoxia, respectively. Similar results were also observed for tube formation (Fig. 6d); there was a decrease in VEGFB levels at normoxia (20% O_2) while all VEGFB levels were upregulated and in a Mg-induced dose-dependent manner under hypoxia (Ctr vs. 4 and 8 mM Mg showed statistically significant differences).

Discussion

Mg-based biomaterials, compared to steel and titanium-related materials, have similar characteristics to bone, including their mechanical properties, density and biodegradability. They are therefore promising materials for orthopaedic applications. After fracture, angiogenesis is one of the early processes associated with tissue healing and can be influenced by its environment (*e.g.*, hypoxia). Hypoxic conditions can be induced and influenced by several parameters around bone fracture and implantation areas, such as inflammation, blood clotting, and highly proliferated cell populations (such as mesenchymal stem cells; MSC). Hypoxia has been proven to affect tissue development and homeostasis [15]. The effects of Mg degradation on the underlying molecular events of angiogenesis still need to be better understood. To study the influence of Mg degradation on angiogenesis, we applied a concentration range of 2-8 mM of Mg ions in our experiments.

Successful (sprouting) angiogenesis involves various stages such as enzymatic degradation of the capillary basement membrane, endothelial cell proliferation as well as their directed migration, endothelial reorganisation of the tube structure (tube formation), vessel fusion, vessel pruning, and pericyte stabilisation [1]. These angiogenesis stages are not completely distinguished from each other. For instance, cell mobility, adhesion and cytoskeletal reorganisation all occur at migration and during the tube formation step. The present findings suggest to some extent that VEGF, the HIF pathways and angiogenic genes are crucial for migration and tubulogenesis when under the influence of hypoxia and Mg degradation products.

Sprouting angiogenesis is initiated when hypoxia is detected in poorly perfused tissues to form new blood vessels to meet the metabolic requirements of parenchymal cells such as skeletal muscle myocytes and neurons in a fracture site. The vitality of HUVECs was assessed *via* the following two different techniques: (1) by measuring the activity of enzymes or oxidoreductases with WST-1 and (2) by determining the mitochondrial membrane potential based on R123 staining. WST-1 is cleaved to soluble formazan dye by the mitochondrial succinate-tetrazolium reductase-NAD^+-NADH system in complex I. However, recent studies indicate that although NADH is responsible for most tetrazolium reduction, NADH is located not only in the mitochondria but also on the cytoplasm membrane, as indicated in Fig. 8 [16]. Moreover, the membrane potential in respiring mitochondria is not always consistent (as judged by the extent of lipophilic ion uptake) with the level of respiration [17]. Therefore, to obtain a more specific assessment of mitochondrial metabolic status, R123 can be applied since it is a lipophilic cation whose cellular accumulation within the mitochondrial matrix is in accordance with the Nernst equation that reflects the ΔΨm (aerobic respiration)-linked ion potential changes via complex III in the electron transport chain (Fig. 8). The increased cellular metabolism measured during normoxia and higher Mg concentrations is probably due to Mg-induced metabolic adaptations including protein and carbohydrate synthesis [18] and ATPase hydrolysis [19]. Many metal ions can perform vital roles in mitochondrial respiration. Ca^{2+}, copper (Cu^{2+}) and iron ($Fe^{2+/3+}$) are functional components of respiratory enzyme complexes I, III and IV. For example, Ca^{2+} regulates cytochrome oxidase complex [20]. Because of its hydration shell, Mg can be a non-competitive antagonist of cations such as Ca^{2+}, Na^+, and K^+ [21]. Mg increases the positively charged inner membrane proton gradient that pumps protons and maintains the energy to drive ATP synthesis by F_0F_1ATPase in the respiratory chain [22]. Consequently, Mg changes the potential gradient according to the electrochemical potential gradient [23]. Hypoxia can attenuate the adaptation of Mg *via* ATPase and its receptor [24]. Moreover, the glycolytic products will be metabolised by anaerobic fermentation, which produces a lower yield of ATP than oxygen-dependent aerobic respiration [25].

Metabolic changes are involved in cellular proliferation and differentiation, and thus, could be important to EC angiogenesis. An increased proliferation was measured with Mg extracts under hypoxia but not under normoxia. A previous study reported $MgSO_4$ (up to 10 mM) can increase the proliferation of endothelial cells [26]. However, this enhanced proliferation was not observed under normoxia only under hypoxia, which suggests the synergistic effects of hypoxia and HIF expression. Another explanation for

this discrepancy can be the form of Mg studied. Indeed, different effects of $MgCl_2$ and Mg extracts were already observed during osteogenesis and osteoclastogenesis, suggesting the higher complexity of the Mg extract composition and properties [27, 28]. The results for the increased ΔΨm under Mg influence are consistent with the hypothesis that mitochondrial activity may play a role in the stimulation of endothelial migration. The stimulated migration by Mg may partially be regulated by the influence of metabolic activity [18]. The elevated ΔΨm in the most motile HUVECs also suggests an increased need for mitochondrial activity, *i.e*., ATP synthesis during migration [29]. Higher Δψm results in greater ATP production and ROS production [30]. Accumulating evidence suggests that ROS functions as a direct signalling molecule in angiogenesis by influencing the HIF pathway and inflammation [31]. Meanwhile, hypoxia can regulate ROS regeneration by inducing eNOS and NADPH oxidases [32]. Since Mg is an adenylate cyclase and cAMP-dependent phosphodiesterase cofactor, the sensitisation to motogenic factors might be dependent on cAMP altered by elevated Mg, which can modulate endothelial migration [33]. Mitochondrial Ca^{2+} uptake, which may be influenced by Mg^{2+}, controls actin cytoskeleton dynamics to affect cell migration [34]. Accordingly, the decreased metabolism in hypoxia suggests that hypoxia can decrease migration due to Mg degradation by potentially suppressing ATPase [35].

Across angiogenesis, VEGFA is the primary regulator when parenchymal cells respond to a hypoxic environment [1]. Under normoxia and with Mg extracts, HUVEC migration exhibited a bell-shaped curve. The same pattern was observed with VEGFB expression, while VEGFA was constantly downregulated. Under hypoxia, migration and VEGFA levels remain constant; however, VEGFB was upregulated. Similarly, under normoxia, tube formation as well as VEGFA and VEGFB levels were downregulated. Nevertheless, under hypoxia, tube formation remained constant while VEGFA and VEGFB levels were upregulated. The HIF pathway is currently proven to be a core regulator of most transcriptional responses to hypoxia and further angiogenic factors [36]. Our results indicate the regulatory roles of VEGFB during hypoxia and Mg degradation and suggest these roles being cellular stage-dependent. Compared to VEGFA, the effects of VEGFB on angiogenesis remain mainly unexplored. The differences in the hypoxia effects on migration and tube formation when influenced by Mg degradation rely on HIF downregulation. Various studies have reported that HIF can upregulate gene and protein expression related to VEGF and VEGFR [37]. VEGFRs can be mediated by HIF *via* the FLT1 promoter or through post-translational mechanisms [38]. Hypoxia downregulated the expression of NOS. Hypoxia attenuated VEGF-stimulated activation of NOS2 and has been noted as a consequence for nitric oxide release in endothelial cells [39]. Other studies contradict these results by showing that hypoxia effects may depend on the cell type [40]. Though extracellular Mg is high, Mg^{2+} can only alter the intracellular Mg^{2+} by transporting Mg^{2+} through ion transporters or channels similar to TRPM7 [41]. CAPN1 can decrease HD-PTP (PTPN23) to influence intracellular Mg^{2+} [42]. Claudins are transmembrane tight junction proteins and directly responsible for forming ion selective channels or pores. Claudin16 was formerly reported to have a critical role in the re-absorption of magnesium [43]. Based on our results, extracellular Mg may promote its influence on angiogenesis *via* influencing CAPN1 and CLD16. Moreover, cell morphology changes contribute to endothelial adhesion and the movement of migration and tube formation stage. Our study indicates the Mg can enhance migration while decreasing tubule formation

by regulating cytoskeleton-related genes such as ANG, VCAM1, EZR and CD9. These results are consistent with previous studies showing that the state of Mg^{2+} is dynamically regulated by actin cytoskeleton rearrangement [44]. Hypoxia was proven to induce actin rearrangement and actin stress fibre assembly in cytoskeletal organisation *via* Rho GTPase signalling [45] and to modify matrix (re)modelling [46]. During endothelial adhesion, growth factors and their interactions with adhesion factors can mediate angiogenesis through similar pathways [47]. Adhesion is primarily mediated through integrins binding to the extracellular matrix (ECM) [48]. For example, integrin β1 regulates angiogenic cell survival and differentiation [49]. Integrins can also directly interact with growth factor receptors, thereby regulating the capacity of integrin-growth-factor-receptor complexes to propagate downstream signalling. For instance, PDGF-, FGF2- and VEGF-induced angiogenesis is related to integrins [50, 51]. VCAM-1 is an endothelial adhesion receptor that can bind to integrins and be regulated by CD9 [52].

The endothelial migration process starts with the ECM and its degradation by collagenases. The ECM is also reported to promote capillary-like tube formation [53]. ECM is produced around cells using components such as glycosaminoglycans, perlecan, aggrecan, fibronectin, laminins, tenascin and collagens [54]. The ECM also serves diverse functions, including being involved in cellular adhesion, migration, proliferation, differentiation and death during vascularisation and bone regeneration [54, 55]. These effects may be through the upregulation of molecules such as TGFβ and by transmitting mechanical stress [56]. ANG can act as a substratum to support endothelial adhesion and induce basement membrane degradation [57]. MMPs, as the most prominent family of ECM enzymes, and inhibitors such as TIMP perform important roles in ECM turnover (*e.g.*, collagen degradation) [58]. MMP is a zinc-containing endopeptidase [59]. Since Mg has a similar radius to Zn^{2+}, some investigations suggest that MMPs can be influenced by the Mg content interfering with Zn^{2+} [60]. IL8 is a chemotactic factor that can promote wound healing [61]. Thus, hypoxia, ECM remodelling and chemotaxis can be new targets in Mg-related regenerative medicine.

Some clinical and epidemiological reports indicate the potency of Mg in the treatment of tumours because of its effects on endothelial proliferation and differentiation. Interesting but less efficient for this application are the pleiotropic and diverging effects on tumour growth [62]. Under normoxia, Mg presents a positive effect on endothelial migration, which is in accordance with a former report [26]. This stimulation was abolished under hypoxia; however, the decreased endothelial migration could be a valuable mechanism for inhibiting tumours by suppressing microvessel formation, which is necessary for tumours to metastasize [63]. Additionally, migration dysfunction induced by Mg could decrease the secretion of angiocrine factors from endothelial cells, which normally promote tumour progression [64]. Nevertheless, tube formation increased by Mg and hypoxia strengthened the beneficial role of Mg to fracture healing as well as its effects on MSC fate, osteogenesis and vascularisation around transplant sites [65].

Conclusion

Taken together, these results indicated that Mg extracts did not interfere with angiogenesis under hypoxia. During wound healing, hypoxia is temporary, but Mg degradation is oxygen-dependant, so it may maintain a relatively decreased oxygen content around the implant. Thus, two hypotheses could be drawn. First, due to the increased proliferation of endothelial cells, increased angiogenesis could be expected. However, due to the experimental time scale and methodology these effects may be dampened. Second, the antagonistic effects of hypoxia and Mg could be associated with preventing angiogenesis from being affected. It should be mentioned that abnormally increased angiogenesis can also be pathological, such as in the case of ocular neovascularisation and haemangiomas. Curiously, one of the first therapeutic uses of Mg implants was for the treatment of cavernous haemangioma in the early 20th century. Nevertheless, the interaction between hypoxia and Mg needs to be further investigated for the development of Mg stents or applications in cardiovascular-, orthopaedic- or tumour-related research. Future work will focus on developing a more complex *in vitro* model (*e.g.*, coculture) to further study angiogenesis and stem cell recruitment.

Table 1. Wound healing gene expression changes under different Mg degradation product concentrations and oxygen conditions. Values for the Mg-treated groups represent the regulation fold compared to hypoxia or the normoxia control. Asterisks with the Mg-treated groups indicate significance compared to the respective control (**P≤0.05, ** P≤0.01,* and **** P≤0.001*). Values for the control groups indicate the relative expression fold of hypoxia and normoxia alone when the expression fold of hypoxia is set into 1. Asterisks for the control group indicate significance compared to the hypoxia control. A slash "/" represents a non-significant change.

Name	Mg-content (mM)	Wound healing	
		5% O_2	20% O_2
Angiogenin (ANG)	Ctr	1.000	0.488***
	2	-3.033**	+1.966**
	4	-4.200**	/
	8	-4.306**	/
Vascular cell adhesion protein 1 (VCAM1)	Ctr	1.000	0.602
	2	-2.393**	/
	4	-2.750**	+2.220**
	8	-2.002**	/
Vascular endothelial growth factor B isoform (VEGFB186)	Ctr	1.000	0.499***
	2	-3.626**	+1.931**
	4	-5.509**	+1.560**
	8	-4.189**	-1.503**
Vascular endothelial growth factor receptor 1 (FLT1)	Ctr	1.000	0.438***
	2	-3.293**	+1.909**
	4	-4.757**	+1.581**
	8	-3.766**	-1.382**

Vascular endothelial growth factor receptor 2 (KDR)	Ctr	1.000	0.546**
	2	-3.647**	+1.819**
	4	-4.892**	+1.445**
	8	-3.998**	/
Transmembrane 4 (CD9)	Ctr	1.000	0.635
	2	-3.616**	+1.851**
	4	-4.89**	/
	8	-4.249**	-1.501*
Ezrin (EZR)	Ctr	1.000	0.445**
	2	-3.975**	+2.067**
	4	-5.629**	/
	8	-2.771**	/
Integrin subunit alpha 2 (ITGA2)	Ctr	1.000	0.725*
	2	-3.330**	+1.681**
	4	-5.707**	/
	8	-4.235**	-1.414**
Integrin subunit alpha M (ITGAM)	Ctr	1.000	0.279*
	2	-2.810**	+3.138*
	4	-2.935**	/
	8	/	/
C-X-C motif ligand 8 (CXCL8, IL8)	Ctr	1.000	0.659
	2	-3.546**	+1.893*
	4	-4.749**	+1.523*
	8	-3.182**	-1.854**
Matrix metallopeptidase 13 (MMP3)	Ctr	1.000	0.248**
	2	-5.321**	+2.706**
	4	-6.037**	+2.722*
	8	-4.378**	/
Tissue inhibitors of metalloproteinase 1 (TIMP1)	Ctr	1.000	0.495*
	2	-4.003**	+1.343**
	4	-5.209**	/
	8	-3.299**	/
Hypoxia inducible factor 1 alpha (HIF1A)	Ctr	1.000	0.539**
	2	-2.536**	+1.448*
	4	-2.618**	/
	8	-2.027**	-1.392*
Hypoxia-inducible factor 2 alpha (HIF2A, EPAS)	Ctr	1.000	0.740
	2	-2.825**	/
	4	-3.175**	/
	8	-2.321**	-1.977**
Fibroblast growth factor (FGF2)	Ctr	1.000	0.518*
	2	-2.683**	+1.861*
	4	-4.040**	/
	8	-3.716**	-1.630*
Interferon gamma (IFNγ)	Ctr	1.000	0.645

	2	-2.611**	+2.250**
	4	-3.312**	/
	8	/	/
Calpain 1 (CAPN1)	Ctr	1.000	0.509*
	2	-3.067**	+1.626*
	4	-5.346**	/
	8	-3.975**	-1.962**
Claudin 16 (CLD16)	Ctr	1.000	0.583
	2	/	/
	4	-3.773**	/
	8	-2.560**	/
Nitric Oxide Synthase 2 (NOS2)	Ctr	1.000	0.323**
	2	-4.614**	+2.974**
	4	-8.479**	-3.697**
	8	/	-5.965*

Table 2. Tube formation gene expression changes under different Mg degradation product concentrations and oxygen conditions. Values for the Mg-treated groups represent the regulation fold compared to hypoxia or the normoxia control. Asterisks with the Mg-treated groups indicate significance compared to the respective control (**P≤0.05, ** P≤0.01,* and **** P≤0.001*). Values for the control groups indicate the relative expression fold of hypoxia and normoxia alone when the expression fold of hypoxia is set into 1. Asterisks for the control group indicate significance compared to the hypoxia control. A slash "/" represents a non-significant change.

Name	Mg-content (mM)	Tube formation	
		5% O_2	20% O_2
Angiogenin (ANG)	Ctr	1.000	0.956
	2	/	+4.283**
	4	/	/
	8	/	/
Vascular endothelial growth factor B isoform (VEGFB186)	Ctr	1.000	3.164**
	2	/	/
	4	/	-1.838**
	8	+2.402*	-1.863**
Vascular endothelial growth factor receptor 1 (FLT1)	Ctr	1.000	3.036*
	2	+2.476*	/
	4	/	-2.974*
	8	+2.521*	-2.027*
Vascular endothelial growth factor receptor 2 (KDR)	Ctr	1.000	4.060**
	2	+2.373*	/
	4	/	-3.997**
	8	+2.322*	-2.229**

Transmembrane 4 (CD9)	Ctr	1.000	2.018
	2	/	/
	4	/	-2.298*
	8	/	-2.750*
Ezrin (EZR)	Ctr	1.000	3.356*
	2	/	/
	4	/	-3.953
	8	/	/
Integrin subunit alpha 3 (ITGA3)	Ctr	1.000	1.101
	2	/	+2.028*
	4	/	/
	8	/	/
C-X-C motif ligand 8 (CXCL8, IL8)	Ctr	1.000	2.164
	2	/	/
	4	/	-1.934*
	8	/	/
Matrix metallopeptidase 13 (MMP3)	Ctr	1.000	0.706
	2	/	/
	4	-2.554*	/
	8	/	/
Tissue inhibitors of metalloproteinase 1 (TIMP1)	Ctr	1.000	2.414
	2	/	/
	4	/	-2.943**
	8	/	-1.867*
Hypoxia inducible factor 1 alpha (HIF1A)	Ctr	1.000	1.478
	2	/	+2.271*
	4	-1.465*	-2.260*
	8	+1.904**	/
Hypoxia-inducible factor 2 alpha (HIF2A, EPAS)	Ctr	1.000	2.039**
	2	/	+2.405**
	4	/	-2.335**
	8	/	/
Fibroblast growth factor (FGF2)	Ctr	1.000	0.429
	2	/	/
	4	/	/
	8	/	/
	Ctr	1.000	2.314
	2	/	/
	4	/	-2.274*
	8	/	/
Calpain 1 (CAPN1)	Ctr	1.000	3.856**
	2	/	/
	4	/	-4.118*
	8	/	-3.485**
Claudin 16 (CLD16)	Ctr	1.000	3.091**

	2	/	/
	4	/	-3.605**
	8	/	-1.990*
Nitric Oxide Synthase 2 (NOS2)	Ctr	1.000	5.473*
	2	/	/
	4	/	-3.697**
	8	/	-5.965*

[1] J.-P.M. Thomas H. Adair, Angiogenesis, San Rafael (CA): Morgan & Claypool Life Sciences; (2010).

[2] T.M. Bedair, M.A. ElNaggar, Y.K. Joung, D.K. Han, Recent advances to accelerate re-endothelialization for vascular stents, Journal of Tissue Engineering 8 (2017) 2041731417731546.

[3] B.P. Eliceiri, D.A. Cheresh, Adhesion events in angiogenesis, Current opinion in cell biology 13(5) (2001) 563-568.

[4] H. Schell, G.N. Duda, A. Peters, S. Tsitsilonis, K.A. Johnson, K. Schmidt-Bleek, The haematoma and its role in bone healing, Journal of Experimental Orthopaedics 4 (2017) 5.

[5] H. Schell, G.N. Duda, A. Peters, S. Tsitsilonis, K.A. Johnson, K. Schmidt-Bleek, The haematoma and its role in bone healing, Journal of experimental orthopaedics 4(1) (2017) 5-5.

[6] D. He, C. Zhuang, C. Chen, S. Xu, X. Yang, C. Yao, J. Ye, C. Gao, Z. Gou, Rational Design and Fabrication of Porous Calcium–Magnesium Silicate Constructs That Enhance Angiogenesis and Improve Orbital Implantation, ACS Biomaterials Science & Engineering 2(9) (2016) 1519-1527.

[7] H. Morii, Overview of skeletal diseases and calcium metabolism in relation to magnesium, New Perspectives in Magnesium Research, Springer2007, pp. 263-265.

[8] E.L. Silva, S.V. Lamaka, D. Mei, M.L. Zheludkevich, The Reduction of Dissolved Oxygen During Magnesium Corrosion, ChemistryOpen 7(8) (2018) 664-668.

[9] S. Prado-Lopez, A. Conesa, A. Arminan, M. Martinez-Losa, C. Escobedo-Lucea, C. Gandia, S. Tarazona, D. Melguizo, D. Blesa, D. Montaner, S. Sanz-Gonzalez, P. Sepulveda, S. Gotz, J.E. O'Connor,

[10] B. Baudin, A. Bruneel, N. Bosselut, M. Vaubourdolle, A protocol for isolation and culture of human umbilical vein endothelial cells, Nature protocols 2(3) (2007) 481-485.

[11] A. Nixon, Y. Jia, C. White, N.A. Bradbury, Determination of the membrane topology of lemur tyrosine kinase 2 (LMTK2) by fluorescence protease protection, American Journal of Physiology - Cell Physiology 304(2) (2013) C164-C169.

[12] A. Baracca, G. Sgarbi, G. Solaini, G. Lenaz, Rhodamine 123 as a probe of mitochondrial membrane potential: evaluation of proton flux through F0 during ATP synthesis, Biochimica et Biophysica Acta (BBA) - Bioenergetics 1606(1) (2003) 137-146.

[13] D. Floryk, J. Houštêk, Tetramethyl Rhodamine Methyl Ester (TMRM) is Suitable for Cytofluorometric Measurements of Mitochondrial Membrane Potential in Cells Treated with Digitonin, Bioscience Reports 19(1) (1999) 27.

[14] R.G. Ronald K. Emaus, John J. Lemasters Rhodamine 123 as a probe of transmembrane potential in isolated rat-liver mitochondria: spectral and metabolic properties.

[15] E.B. Rankin, A.J. Giaccia, E. Schipani, A Central Role for Hypoxic Signaling in Cartilage, Bone, and Hematopoiesis, Current osteoporosis reports 9(2) (2011) 46-52.

[16] F. Haag, S. Adriouch, A. Braß, C. Jung, S. Möller, F. Scheuplein, P. Bannas, M. Seman, F. Koch-Nolte, Extracellular NAD and ATP: Partners in immune cell modulation, Purinergic Signalling 3(1) (2007) 71.

[17] D. Kell, P. John, Continuous monitoring of the electrical potential across energy-transducing membranes using ion-selective electrodes Application to submitochondrial particles and chromatophores, FEBS letters 86(2) (1978) 294-298.

[18] F.I. Wolf, A. Cittadini, Magnesium in cell proliferation and differentiation, Frontiers in bioscience : a journal and virtual library 4 (1999) D607-17.

[19] K.L. West, E.L. Meczes, R. Thorn, R.M. Turnbull, R. Marshall, C.A. Austin, Mutagenesis of E477 or K505 in the B' domain of human topoisomerase II beta increases the requirement for magnesium ions during strand passage, Biochemistry 39(6) (2000) 1223-33.

[20] T. Vygodina, A. Kirichenko, A.A. Konstantinov, Direct regulation of cytochrome c oxidase by calcium ions, PloS one 8(9) (2013) e74436.

[21] W. Jahnen-Dechent, M. Ketteler, Magnesium basics, Clin Kidney J 5(Suppl 1) (2012) i3-i14.

[22] L.B. Chen, Mitochondrial Membrane Potential in Living Cells, Annual Review of Cell Biology 4(1) (1988) 155-181.

[23] M. Huang, A.K.S. Camara, D.F. Stowe, F. Qi, D.A. Beard, Mitochondrial Inner Membrane Electrophysiology Assessed by Rhodamine-123 Transport and Fluorescence, Annals of biomedical engineering 35(7) (2007) 1276-1285.

[24] V.A. Lakunina, K.M. Burnysheva, V.A. Mitkevich, A.A. Makarov, I.Y. Petrushanko, Changes in the receptor function of Na,K-ATPase during hypoxia and ischemia, Molecular Biology 51(1) (2017) 148-154.

[25] P.R. Rich, The molecular machinery of Keilin's respiratory chain, Biochemical Society transactions 31(Pt 6) (2003) 1095-105.

[26] J.A.M. Maier, D. Bernardini, Y. Rayssiguier, A. Mazur, High concentrations of magnesium modulate vascular endothelial cell behaviour in vitro, Biochimica et Biophysica Acta (BBA) - Molecular Basis of Disease 1689(1) (2004) 6-12.

[27] A. Burmester, B. Luthringer, R. Willumeit, F. Feyerabend, Comparison of the reaction of bone-derived cells to enhanced MgCl2-salt concentrations, Biomatter 4(1) (2014) e967616.

[28] L. Wu, F. Feyerabend, A.F. Schilling, R. Willumeit-Römer, B.J. Luthringer, Effects of extracellular magnesium extract on the proliferation and differentiation of human osteoblasts and osteoclasts in coculture, Acta biomaterialia 27 (2015) 294-304.

[29] L.V. Johnson, M.L. Walsh, B.J. Bockus, L.B. Chen, Monitoring of relative mitochondrial membrane potential in living cells by fluorescence microscopy, The Journal of Cell Biology 88(3) (1981) 526-535.

[30] D.B. Zorov, M. Juhaszova, S.J. Sollott, Mitochondrial reactive oxygen species (ROS) and ROS-induced ROS release, Physiological reviews 94(3) (2014) 909-50.

[31] M. Ushio-Fukai, Y. Nakamura, Reactive Oxygen Species and Angiogenesis: NADPH Oxidase as Target for Cancer Therapy, Cancer letters 266(1) (2008) 37-52.

[32] E. Herrera, B. J Krause, G. Ebensperger, V. Reyes, P. Casanello, M. Parra-Cordero, A. Llanos, The placental pursuit for an adequate oxidant balance between the mother and the fetus, 2014.

[33] S.F. Hackett, Z. Friedman, P.A. Campochiaro, Cyclic 3',5'-adenosine monophosphate modulates vascular endothelial cell migration in vitro, Cell biology international reports 11(4) (1987) 279-87.

[34] J. Prudent, N. Popgeorgiev, R. Gadet, M. Deygas, R. Rimokh, G. Gillet, Mitochondrial Ca2+ uptake controls actin cytoskeleton dynamics during cell migration, 6 (2016) 36570.

[35] G.A. Gusarova, H.E. Trejo, L.A. Dada, A. Briva, L.C. Welch, R.B. Hamanaka, G.M. Mutlu, N.S. Chandel, M. Prakriya, J.I. Sznajder, Hypoxia Leads to Na,K-ATPase Downregulation via Ca(2+) Release-Activated Ca(2+) Channels and AMPK Activation, Molecular and Cellular Biology 31(17) (2011) 3546-3556.

[36] B.L. Krock, N. Skuli, M.C. Simon, Hypoxia-Induced Angiogenesis: Good and Evil, Genes & Cancer 2(12) (2011) 1117-1133.

[37] M. Shibuya, Vascular Endothelial Growth Factor (VEGF) and Its Receptor (VEGFR) Signaling in Angiogenesis: A Crucial Target for Anti- and Pro-Angiogenic Therapies, Genes & Cancer 2(12) (2011) 1097-1105.

[38] H.-P. Gerber, F. Condorelli, J. Park, N. Ferrara, Differential transcriptional regulation of the two vascular endothelial growth factor receptor genes Flt-1, but not Flk-1/KDR, is up-regulated by hypoxia, Journal of Biological Chemistry 272(38) (1997) 23659-23667.

[39] B. Olszewska-Pazdrak, T.W. Hein, P. Olszewska, D.H. Carney, Chronic hypoxia attenuates VEGF signaling and angiogenic responses by downregulation of KDR in human endothelial cells, American Journal of Physiology-Cell Physiology 296(5) (2009) C1162-C1170.

[40] H.H. Marti, W. Risau, Systemic hypoxia changes the organ-specific distribution of vascular endothelial growth factor and its receptors, Proceedings of the National Academy of Sciences 95(26) (1998) 15809-15814.

[41] S. Castiglioni, A. Cazzaniga, V. Trapani, C. Cappadone, G. Farruggia, L. Merolle, F.I. Wolf, S. Iotti, J.A.M. Maier, Magnesium homeostasis in colon carcinoma LoVo cells sensitive or resistant to doxorubicin, Scientific Reports 5 (2015) 16538.

[42] S. Castiglioni, J.A. Maier, The tyrosine phosphatase HD-PTP (PTPN23) is degraded by calpains in a calcium-dependent manner, Biochem Biophys Res Commun 421(2) (2012) 380-3.

[43] J. Hou, D.A. Goodenough, Claudin-16 and claudin-19 function in the thick ascending limb, Current opinion in nephrology and hypertension 19(5) (2010) 483-8.

[44] S.Y. Jeong, S.Y. Shin, H.-S. Kim, C.-D. Bae, D.-Y. Uhm, M.-K. Park, S. Chung, Regulation of magnesium-inhibited cation current by actin cytoskeleton rearrangement, Biochemical and Biophysical Research Communications 339(3) (2006) 810-815.

[45] A. Zieseniss, Hypoxia and the modulation of the actin cytoskeleton – emerging interrelations, Hypoxia 2 (2014) 11-21.

[46] F. Baffert, Y. Usson, L. Tranqui, Effects of prolonged exposure to hypoxia on morphological changes of endothelial cells plated on fibrin gel, European Journal of Cell Biology 80(1) (2001) 78-86.

[47] S. Kim, M. Harris, J.A. Varner, Regulation of integrin αvβ3-mediated endothelial cell migration and angiogenesis by integrin α5β1 and protein kinase A, Journal of Biological Chemistry 275(43) (2000) 33920-33928.

[48] C.A. Reinhart-King, Endothelial cell adhesion and migration, Methods in enzymology 443 (2008) 45-64.

[49] T.S. Li, H. Ito, M. Hayashi, A. Furutani, M. Matsuzaki, K. Hamano, Cellular expression of integrin-beta 1 is of critical importance for inducing therapeutic angiogenesis by cell implantation, Cardiovascular research 65(1) (2005) 64-72.

[50] E. Borges, Y. Jan, E. Ruoslahti, Platelet-derived growth factor receptor β and vascular endothelial growth factor receptor 2 bind to the β3integrin through its extracellular domain, Journal of Biological Chemistry 275(51) (2000) 39867-39873.

[51] G.H. Mahabeleshwar, W. Feng, K. Reddy, E.F. Plow, T.V. Byzova, Mechanisms of integrin-vascular endothelial growth factor receptor cross-activation in angiogenesis, Circ Res 101(6) (2007) 570-80.

[52] M. Schlesinger, G. Bendas, Vascular cell adhesion molecule-1 (VCAM-1)--an increasing insight into its role in tumorigenicity and metastasis, International journal of cancer 136(11) (2015) 2504-14.

[53] F. Berthod, L. Germain, N. Tremblay, F.A. Auger, Extracellular matrix deposition by fibroblasts is necessary to promote capillary-like tube formation in vitro, Journal of cellular physiology 207(2) (2006) 491-8.

[54] M. Matusiewicz, Extracellular Matrix Remodeling, in: M. Schwab (Ed.), Encyclopedia of Cancer, Springer Berlin Heidelberg, Berlin, Heidelberg, 2011, pp. 1362-1365.

[55] E.H. Chung, M. Gilbert, A.S. Virdi, K. Sena, D.R. Sumner, K.E. Healy, Biomimetic artificial ECMs stimulate bone regeneration, Journal of Biomedical Materials Research Part A 79A(4) (2006) 815-826.

[56] B. Hinz, The extracellular matrix and transforming growth factor-β1: Tale of a strained relationship, Matrix Biology 47 (2015) 54-65.

[57] F. Soncin, Angiogenin supports endothelial and fibroblast cell adhesion, Proc Natl Acad Sci U S A 89(6) (1992) 2232-6.

[58] J.A. Jones, A.K. McNally, D.T. Chang, L.A. Qin, H. Meyerson, E. Colton, I.L.K. Kwon, T. Matsuda, J.M. Anderson, Matrix metalloproteinases and their inhibitors in the foreign body reaction on biomaterials, Journal of Biomedical Materials Research Part A 84A(1) (2008) 158-166.

[59] L. Ravanti, V.M. Kahari, Matrix metalloproteinases in wound repair (review), International journal of molecular medicine 6(4) (2000) 391-407.

[60] H. Yue, J.-D. Lee, H. Shimizu, H. Uzui, Y. Mitsuke, T. Ueda, Effects of magnesium on the production of extracellular matrix metalloproteinases in cultured rat vascular smooth muscle cells, Atherosclerosis 166(2) (2003) 271-277.

[61] H.O. Rennekampff, J.F. Hansbrough, V. Kiessig, C. Dore, M. Sticherling, J.M. Schroder, Bioactive interleukin-8 is expressed in wounds and enhances wound healing, The Journal of surgical research 93(1) (2000) 41-54.

[62] F.I. Wolf, A.R.M. Cittadini, J.A.M. Maier, Magnesium and tumors: Ally or foe?, Cancer Treatment Reviews 35(4) (2009) 378-382.

[63] A.E. German, T. Mammoto, E. Jiang, D.E. Ingber, A. Mammoto, Paxillin controls endothelial cell migration and tumor angiogenesis by altering neuropilin 2 expression, Journal of Cell Science 127(8) (2014) 1672-1683.

[64] N. Maishi, K. Hida, Tumor endothelial cells accelerate tumor metastasis, Cancer science 108(10) (2017) 1921-1926.

[65] B.J.C. Luthringer, R. Willumeit-Römer, Effects of magnesium degradation products on mesenchymal stem cell fate and osteoblastogenesis, Gene 575(1) (2016) 9-20.

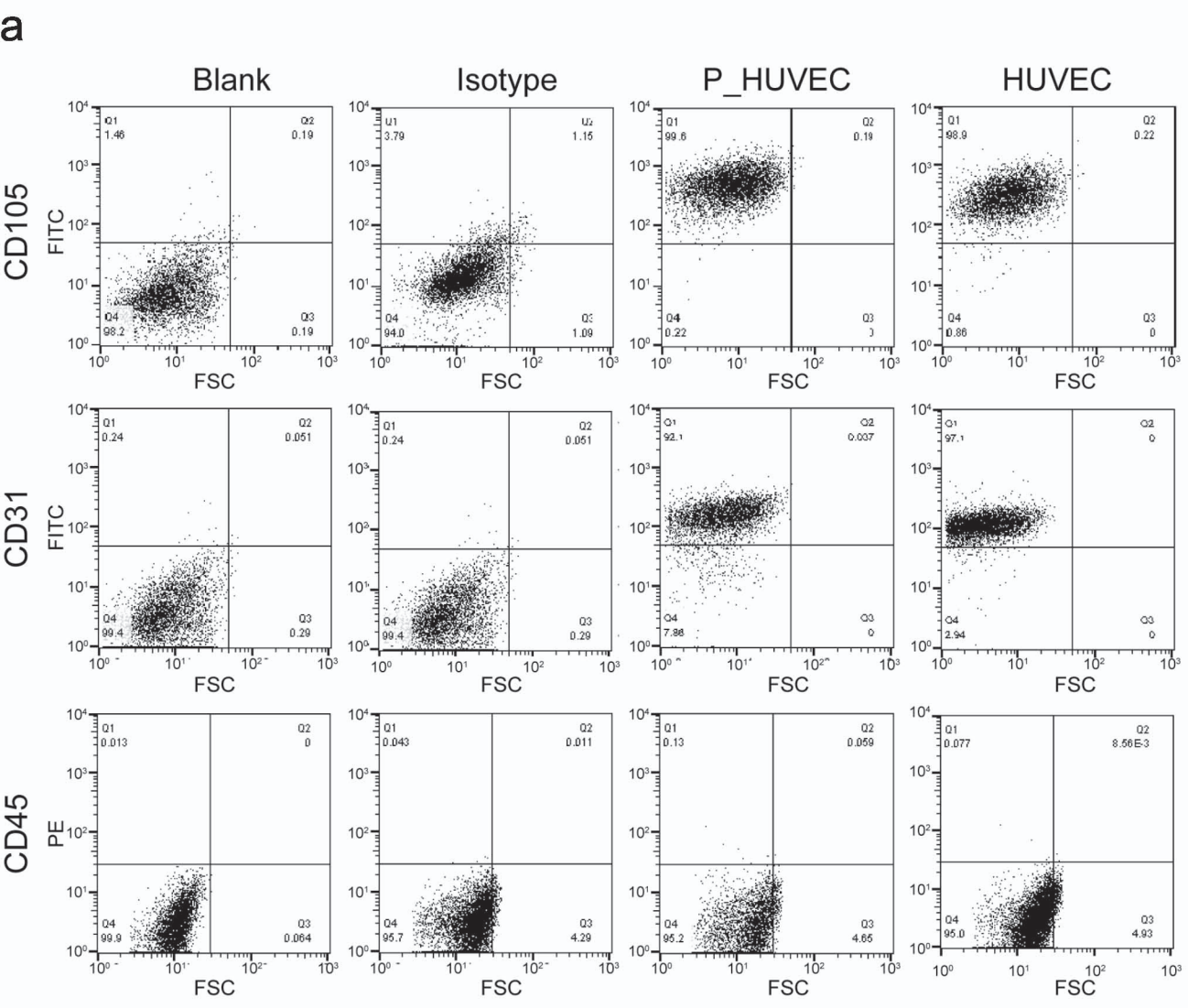
a
Blank
Isotype
P_HUVEC
HUVEC
CD105
CD31
CD45
FITC
PE
FSC
Q1 1.46
Q2 0.19
Q4 98.2
Q3 0.19
Q1 3.79
Q2 1.15
Q4 94.0
Q3 1.09
Q1 99.6
Q2 0.19
Q4 0.22
Q3
Q1 98.9
Q2 0.22
Q4 0.86
Q3 0
Q1 0.24
Q2 0.051
Q4 99.4
Q3 0.29
Q1 0.24
Q2 0.051
Q4 99.4
Q3 0.29
Q1 92.1
Q2 0.037
Q4 7.86
Q3 0
Q1 97.1
Q2 0
Q4 2.94
Q3 0
Q1 0.013
Q2 0
Q4 99.9
Q3 0.064
Q1 0.043
Q2 0.011
Q4 95.7
Q3 4.29
Q1 0.13
Q2 0.059
Q4 95.2
Q3 4.65
Q1 0.077
Q2 8.56E-3
Q4 95.0
Q3 4.93
b
Positive cell (%)
***
***
100
80
60
40
4
3
2
1
0
CD105
CD31
CD45
Isotype
P_HUVEC
HUVEC

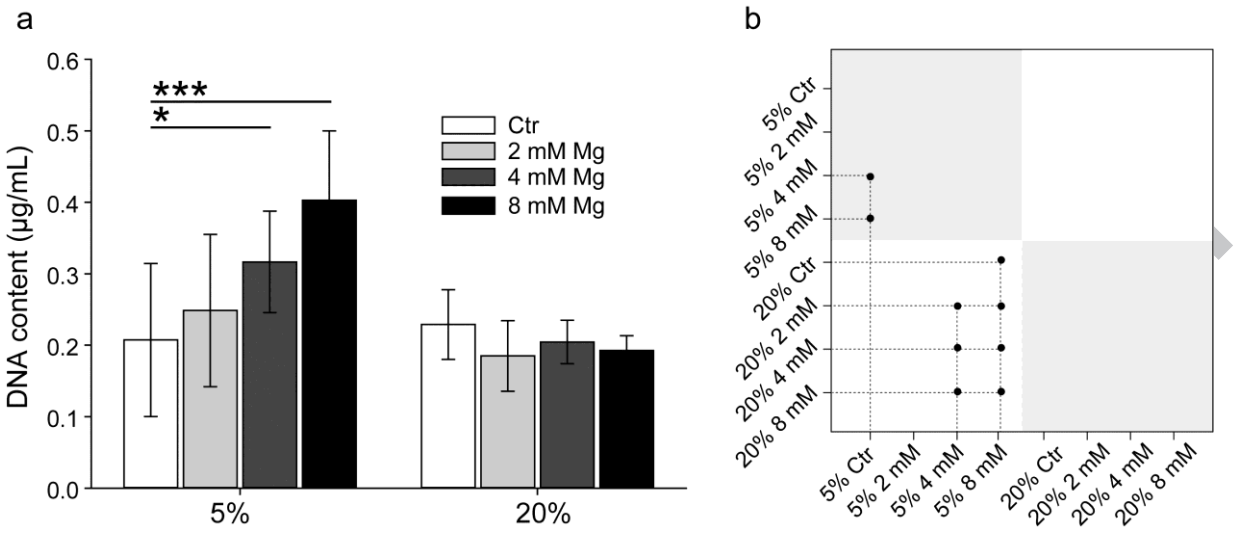
a
DNA content (µg/mL)
0.6
0.5
0.4
0.3
0.2
0.1
0.0
***
*
Ctr
2 mM Mg
4 mM Mg
8 mM Mg
5%
20%
b
5% Ctr
5% 2 mM
5% 4 mM
5% 8 mM
20% Ctr
20% 2 mM
20% 4 mM
20% 8 mM

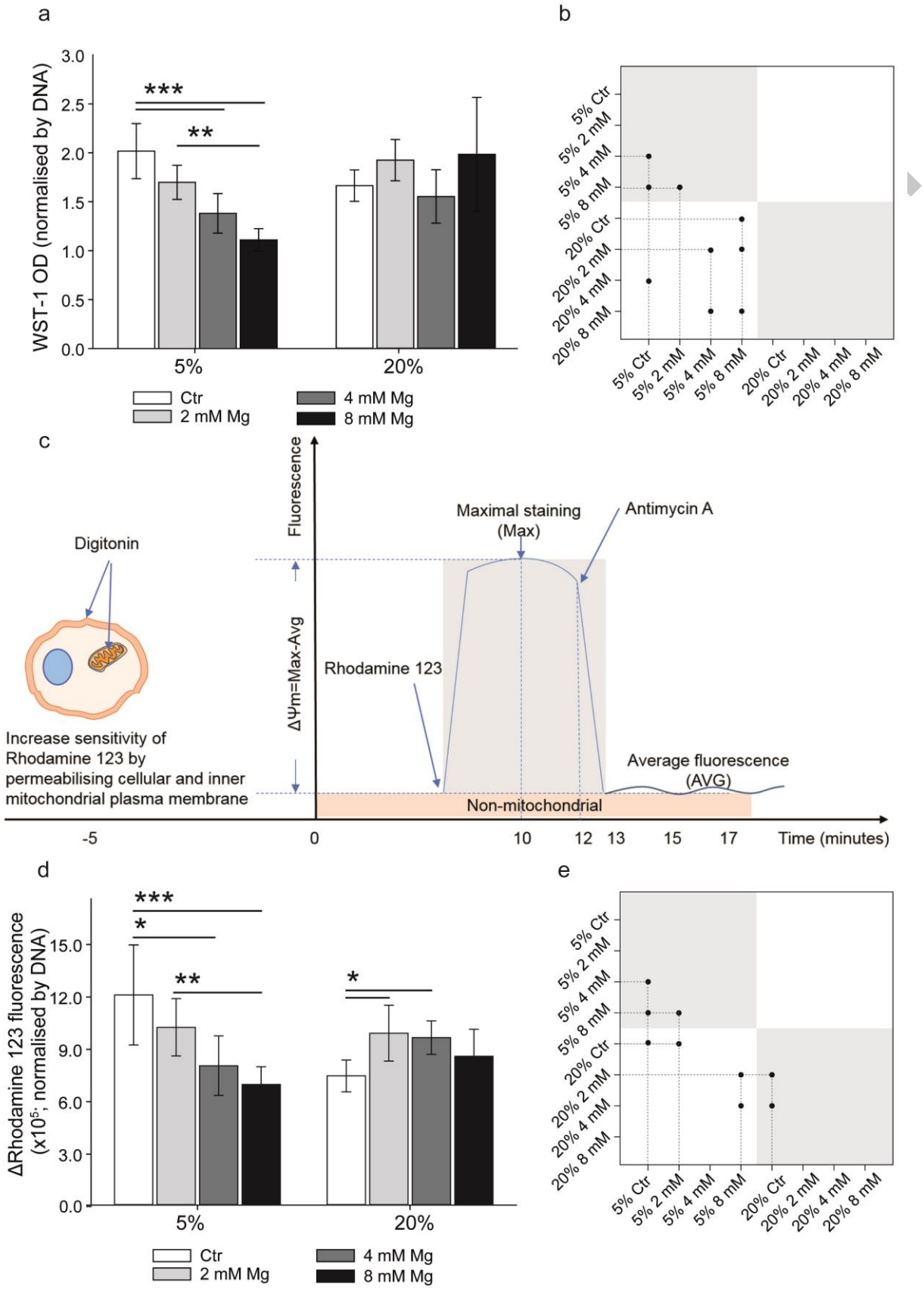
a
WST-1 OD (normalised by DNA)
3.0
2.5
2.0
1.5
1.0
0.5
0.0
***
**
5%
20%
Ctr
2 mM Mg
4 mM Mg
8 mM Mg
b
5% Ctr
5% 2 mM
5% 4 mM
5% 8 mM
20% Ctr
20% 2 mM
20% 4 mM
20% 8 mM
c
Digitonin
Increase sensitivity of Rhodamine 123 by permeabilising cellular and inner mitochondrial plasma membrane
Fluorescence
ΔΨm=Max-Avg
Maximal staining (Max)
Antimycin A
Rhodamine 123
Average fluorescence (AVG)
Non-mitochondrial
-5
0
10
12
13
15
17
Time (minutes)
d
ΔRhodamine 123 fluorescence (x10⁵; normalised by DNA)
15.0
12.0
9.0
6.0
3.0
0.0
***
*
**
*
5%
20%
Ctr
2 mM Mg
4 mM Mg
8 mM Mg
e
5% Ctr
5% 2 mM
5% 4 mM
5% 8 mM
20% Ctr
20% 2 mM
20% 4 mM
20% 8 mM

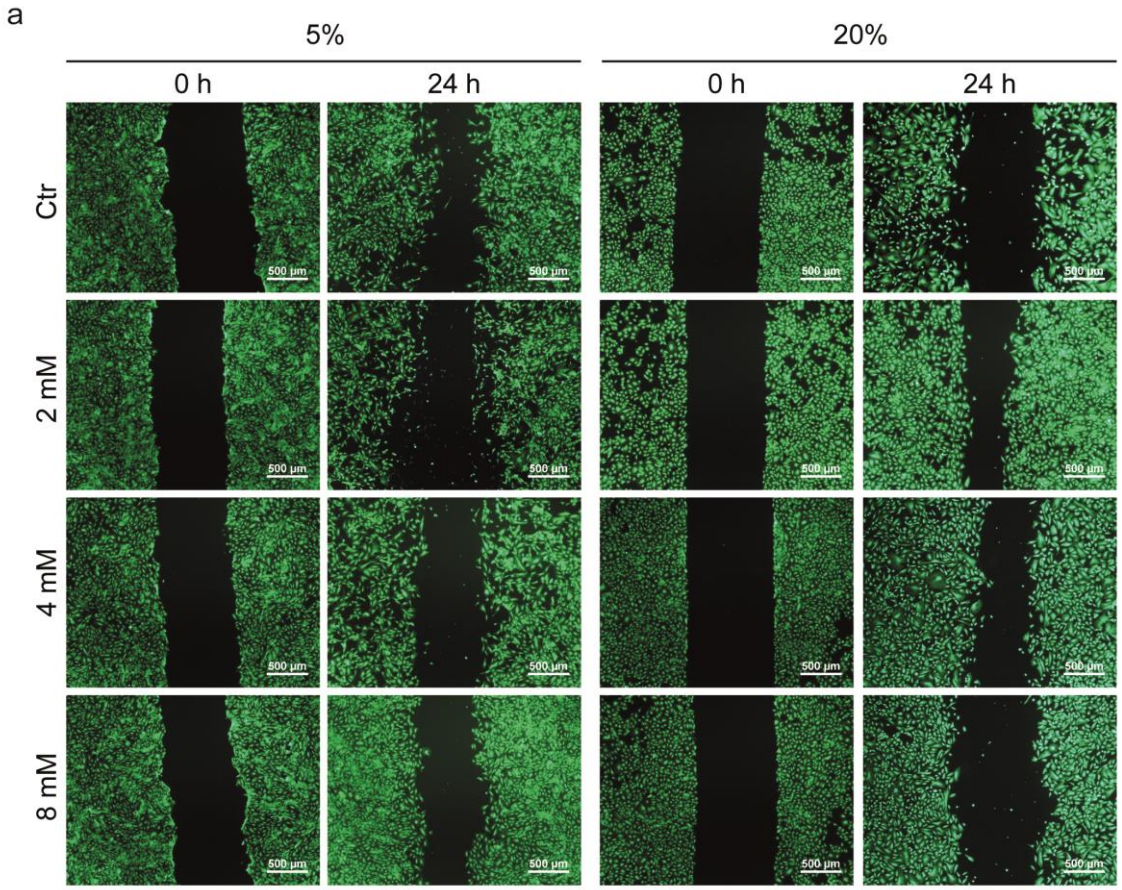
a
5%
20%
0 h
24 h
0 h
24 h
Ctr
2 mM
4 mM
8 mM
500 μm

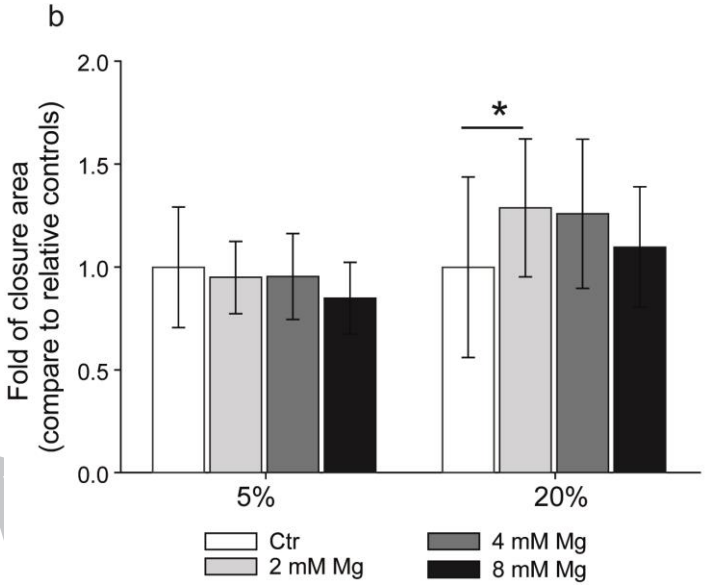
b
Fold of closure area
(compare to relative controls)
2.0
1.5
1.0
0.5
0.0
*
5%
20%
Ctr
2 mM Mg
4 mM Mg
8 mM Mg

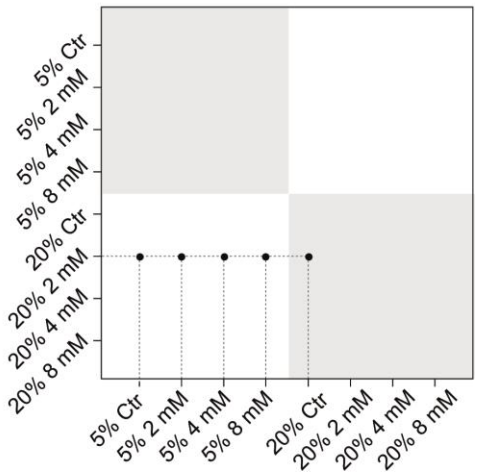
c
5% Ctr
5% 2 mM
5% 4 mM
5% 8 mM
20% Ctr
20% 2 mM
20% 4 mM
20% 8 mM

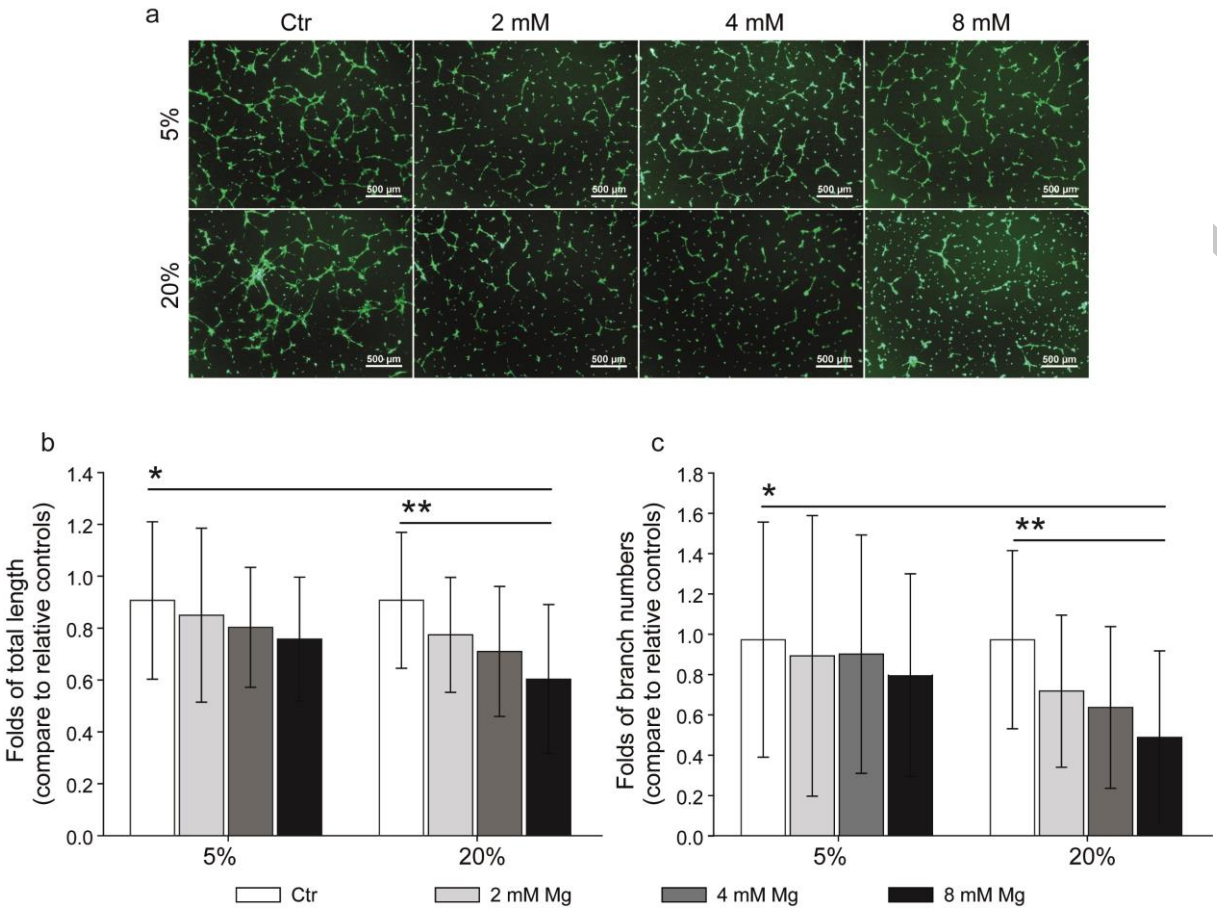

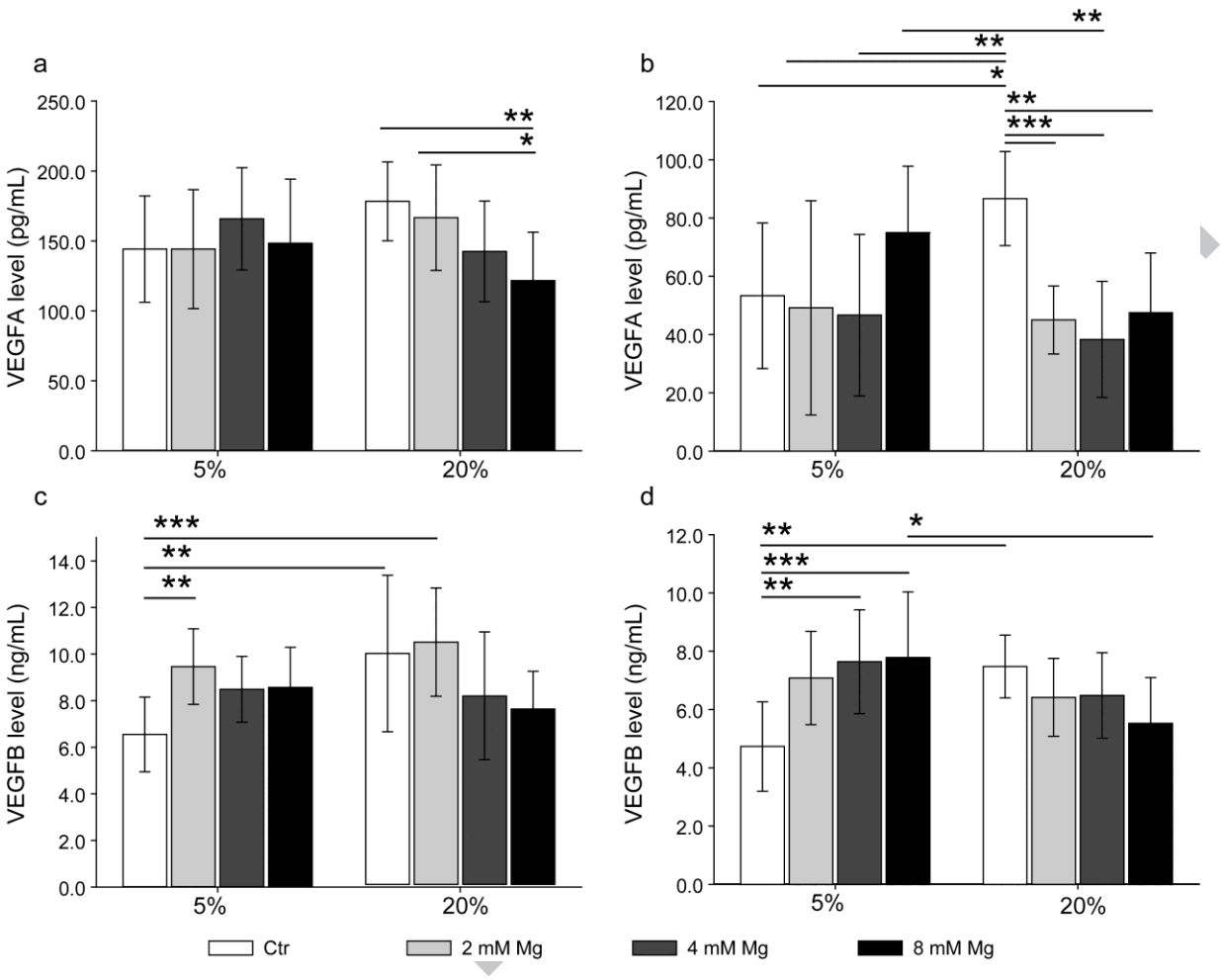

a

	5%	20%
Proliferation	↗	→
Metabolic activity	↘	→
Δψm	↘	→

EARLY

	5%				20%			
Migration	→				↘			
VEGFA	→				↘			
VEGFB	↗				↘			
Gene level		⇧	⇩	⇦⇨		⇧	⇩	⇦⇨
	2 mM	0%	90%	10%	2 mM	80%	0%	20%
	4 mM	0%	95%	5%	4 mM	30%	5%	65%
	8 mM	0%	80%	20%	8 mM	0%	50%	50%
	Total	**0%**	**88%**	**12%**	**Total**	**37%**	**18%**	**45%**

LATE

	5%				20%			
Tube formation	→				↘			
VEGFA	↗				↘			
VEGFB	↗				↘			
Gene level		⇧	⇩	⇦⇨		⇧	⇩	⇦⇨
	2 mM	10%	0%	90%	2 mM	20%	0%	80%
	4 mM	0%	10%	90%	4 mM	0%	65%	35%
	8 mM	20%	0%	80%	8 mM	0%	40%	60%
	Total	**10%**	**3%**	**87%**	**Total**	**7%**	**35%**	**58%**

b

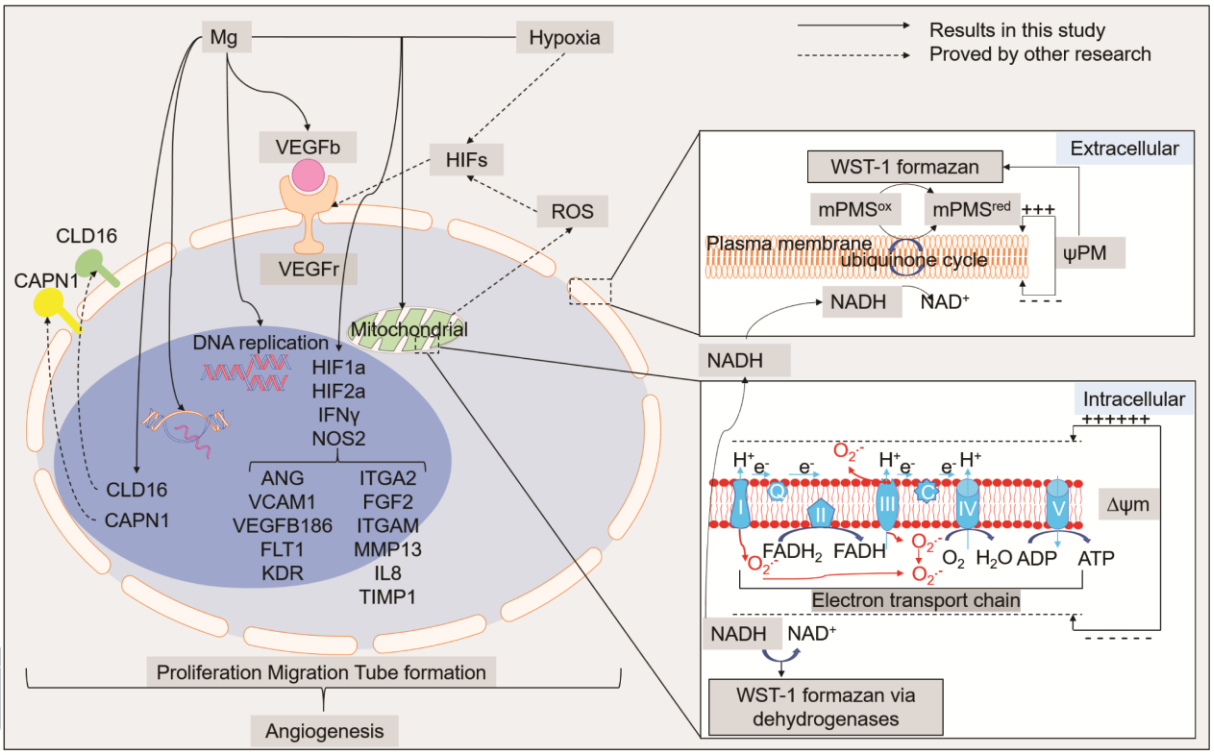

Fig. 1 HUVEC characterisation: (a) mock flow cytometry dot-plots of purchased HUVEC (P_HUVEC) and isolated HUVEC immunophenotyping. CD105 and CD31 were selected as positive markers and CD 45 as negative one (b) summary of surface markers of isotypes control, purchased HUVEC (P_HUVEC) and isolated HUVEC, identified by flow cytometry (triplicate of 3 independent experiments). Morphology "cobblestone" graph is available in Supplementary Fig. 1. Significant difference (ANOVA test) between two groups is indicated by an asterisk (****P*≤0.001).

Fig. 2 Proliferation of HUVEC indicated by DNA contents. **(a)** Significance between treatments was tested by ANOVA and indicated by an asterisk (**P≤0.05 and* ****P≤0.001*). (b) Post-hoc multiple comparisons between each treatments. Solid dot represents significant difference.

Fig. 3 Metabolic activity of HUVEC measured by WST-1 assay and R123 fluorescence quenching. (a)(d) Significance between treatments was tested by ANOVA and indicated by an asterisk (**P≤0.05, **P≤0.01* and ****P≤0.001*). (c) **Principle and procedure overview of** ΔΨM tests. (b)(e) Post-hoc multiple comparisons between each treatments. Solid dot represents significant difference.

Fig. 4 Wound healing closure of HUVEC in presence of Mg degradation products under hypoxia (5% O_2) or normoxia (20% O_2). (a) Pictures at 0 h and 24 h. (b) Values represent the no-cell-area difference between 24 h and 0 h, further normalised to relative controls. Significance between treatments was tested by ANOVA and indicated by an asterisk (**P≤0.05*). (c) Post-hoc multiple comparisons between each treatments. Solid dot represents significant difference.

Fig. 5 Tube formation of HUVEC in Magnesium degradation products. After 6 hours, tubes were stained with Calcein AM and images were taken with an inverted microscope (a). Thanks to Image J with Angiogenesis Analyser Plugin, the total length of tubes (b) and the number of branches (c) were calculated. Significance between treatments was tested by ANOVA and indicated by an asterisk (**P≤0.05, **P≤0.01, and ****P≤0.001*).

Fig. 6 VEGFA and VEGFB level secreted in wound healing (a and c, respectively) and tube formation (b and d, respectively) assays. Asterisk represents significant difference between Mg groups and controls with same oxygen setting (**P≤0.05, **P≤0.01)* in ANOVA test.

Fig. 7 Summary of results (a) and schematic overview of HUVEC angiogenesis and effects of Mg and oxygen contents (b). Abbreviations: magnesium (Mg); vascular endothelial growth factor beta (VEGFB); vascular endothelial growth factor receptor (VEGFR); C-X-C motif chemokine 8 (IL8); fibroblast growth factor basic (FGFb); vascular endothelial growth factor receptor 2 (KDR); hypoxia-inducible factors (HIFs); reactive oxygen species (ROS); plasma membrane surface potential (ψPM); mitochondrial membrane potential (Δψm); 1-methoxy-5-methyl-phenazinium methyl sulfate oxidative ($mPMS^{ox}$): an intermediate electron acceptor.


Tube formation
Increased concentration Mg
Proliferation
Migration
(wound healing)
5% O2
20% O2
5% O2
20% O2
5% O2
20% O2